AGU Fall 2018
T43E-0458

The February 2018 Mw 7.2 Pinotepa Earthquake in Mexico Ruptured a Small Patch of the Oaxaca Megathrust

Eric J. Fielding(fielding@jpl.nasa.gov)[1], J. Alejandro González-Ortega[2], Baptiste Gombert[3], Zacharie Duputel[4], Cunren Liang[5], Romain Jolivet[6], David Bekaert[1], Jean-Paul Ampuero[5,7]

[1]Jet Propulsion Laboratory, California Institute of Technology, California, USA; [2]CICESE, Ensenada, Mexico; [3]Earth Sciences, University of Oxford, UK; [4]IPGS, Université de Strasbourg/EOST, CNRS, Strasbourg Cedex, France; [5]Seismological Laboratory, California Institute of Technology, California, USA; [6]École Normale Supérieure, Paris, France; [7]Université Côte d'Azur, IRD, CNRS, Géoazur, France

National Aeronautics and Space Administration

Introduction

The subduction zone of the Cocos Plate beneath Southern Mexico has major variations in the megathrust geometry and behavior. The subduction segment beneath the Oaxaca state of Mexico has relatively frequent large earthquakes on the shallow part of the megathrust and within the subducting slab, and it also has large aseismic slow-slip events. The slab geometry under Oaxaca includes part of the subhorizontal "flat-slab" zone extending far from the trench beneath southern Mexico and the beginning of its transition to more regular subduction geometry to the southeast. We study the rupture of the 16 February 2018 Mw 7.2 Pinotepa earthquake near Pinotepa Nacional in Oaxaca that was a thrust event on the subduction interface. The Pinotepa earthquake was about 350 km away from the 8 September 2017 Mw 8.2 Tehuantepec earthquake in the subducting slab offshore Oaxaca and Chiapas; it was in an area of Coulomb stress decrease from the M8.2 quake, so it seems unlikely to be a regular aftershock and was not triggered by the static stress change.

Geodetic measurements from interferometric analysis of synthetic aperture radar (InSAR) and time-series analysis of GPS station data constrain finite-fault slip models for the M7.2 Pinotepa earthquake. We analyzed InSAR data from Copernicus Sentinel-1A and -1B satellites and JAXA ALOS-2 satellite. Our Bayesian (AlTar) static slip model for the Pinotepa earthquake shows all of the slip confined to a very small (10-20 km diameter) rupture, similar to some early seismic waveform fits. The Pinotepa earthquake ruptured a portion of the Cocos megathrust that has been previously mapped as partially coupled and shows that at least small asperities in that zone of the subduction interface are fully coupled and fail in high-stress drop earthquakes. The previous 2012 Mw 7.4 Ometepec earthquake is another example of asperity in the partially coupled zone but was not imaged by InSAR so the rupture extent is not so well constrained. The preliminary NEIC epicenter for the Pinotepa earthquake was about 40 km away (NE) from the rupture imaged by InSAR, but the NEIC updated epicenter and Mexican SSN location are closer. Preliminary analysis of GPS data after the Pinotepa earthquake indicates rapid afterslip on the megathrust in the region of coseismic slip. Atmospheric noise masks the postseismic signal on early InSAR data.

Southeast Mexico subduction zone and 2017–2018 large earthquakes

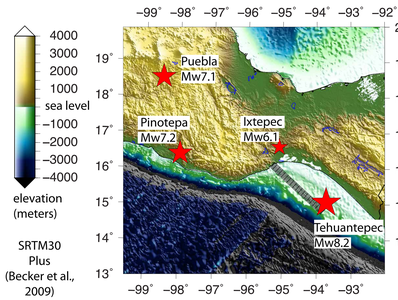

Figure 1.
Regional map of southeastern Mexico with epicentral locations of large earthquakes in September 2017 and February 2018 (red stars). Sequence started with Mw 8.2 Tehuantepec Earthquake, a normal rupture of the subducting slab beneath Gulf of Tehuantepec offshore Chiapas on 8 September. The Mw 7.1 Puebla Earthquake ruptured the slabe beneath Puebla state on 19 September, and the Mw 6.1 Ixtepec Earthquake struck in the upper plate near the city of Ixtepec in Oaxaca on 23 September 2017. These events were followed by the Mw 7.2 Pinotepa Earthquake on 16 February 2018, rupturing part of the megathrust beneath Oaxaca state. Coulomb stress change calculations using Tehuantepec slip model (Gombert et al., 2017) shows that Pinotepa rupture was not encouraged by static stress change from Tehuantepec quake. Epicenters from the USGS NEIC. Shaded relief topography from SRTM30 plus (Becker et al., 2009).

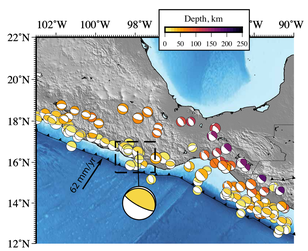

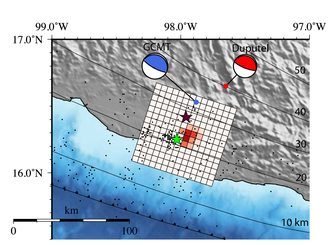

Figure 2. (*Left*) Seismicity from 1976 to 2018 in southeast Mexico showing GCMT solutions for events with Mw>=6.0, color coded by depth. Most shallow (depth < 30 km) thrust events are on megathrust interface while most deeper events are within subducting Cocos Plate slab. Centroid moment tensor for 2018 Pinotepa earthquake shown with large beachball. Bathymetry and topography from SRTM30 Plus (Becker et al., 2009) v11. Box shows location of map on right. (*Right*) Two moment tensor solutions for Pinotepa earthquake with their estimated centroid locations from Global CMT and this study (Duputel W-phase). Rectangular outline shows location of model fault with slip model from AlTar inversion. Black dots are Mexican SSN aftershock epicenters. Dark red star is USGS NEIC revised epicenter and green star is Mexican SSN epicenter location for Pinotepa earthquake. Thin black lines are contours on Slab2.0 megathrust depth model from Hayes et al. (2018).

National Aeronautics and Space Administration

Jet Propulsion Laboratory
California Institute of Technology
Pasadena, California

www.nasa.gov

Mw 7.2 Pinotepa Earthquake on megathrust

Fault geometry

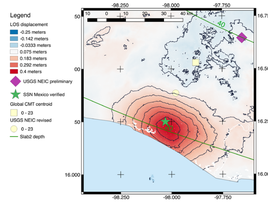

Figure 3. Map of area around 16 February 2018 M7.2 Pinotepa earthquake with Sentinel-1A/B ascending track 005 interferogram (20180205–0217) shown in color corresponding to line-of-sight (LOS) displacements, with 5 cm contours as thin black lines. Second Sentinel-1 scene was acquired less than two hours after the earthquake and automatically downloaded and processed by the Advanced Rapid Imaging and Analysis (ARIA) data system. Red areas moved up or west in this plot and "bulls-eye" pattern shows location of uplift due to thrust slip at depth. Epicenters shown: USGS NEIC preliminary (magenta diamond), USGS NEIC revised (yellow circle), and Mexican SSN "verificado" (green star) epicenters and Global CMT centroid (yellow square). Early NEIC locations from teleseismic arrivals at global networks were off by up to 40 km, as previously observed for southern Mexico (Hjörleifsdóttir et al., 2016). Mexican SSN and revised USGS location using regional data much closer to InSAR signal.

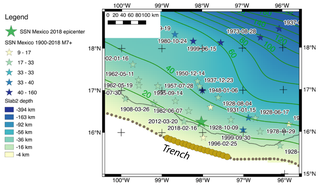

Figure 4. Slab2.0 database (Hayes et al., 2018) for Oaxaca-Guerrero area (colors) used for generating model faults. Large brown circles show top (trench) location of slab section used for fault model "1.2" with 15x15 km patches.
Stars show locations of M>=7 earthquakes in the SSN Mexico catalog 1901–2018, color-coded by depth with date labels. Older events have uncertain depths and some are set to nominal 33 km. Large green star shows SSN 2018 Pinotepa epicenter. Most deeper events are intra-slab normal events. Events shallower than 25 km are mostly megathrust events. This subduction zone has many M7–7.5 quakes in last century and is in transition between flat-slab of Guerrero and steeper slab of eastern Oaxaca and Chiapas.

AlTar slip distribution inversion with InSAR + GPS

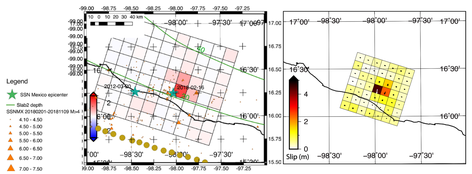

Figure 5. (*Left*) Map of mean of 150,000 samples of slip posterior distribution functions (PDF) from Bayesian AlTar inversion (Minson et al., 2013) for Pinotepa earthquake slip on model v1.2 fault with 15x15 km patches. Input is uniform prior on dip-slip only (no along-strike slip) between (-0.1–20 m) and three Sentinel-1 interferograms and one ALOS-2 interferogram with data covariances estimated from data (Figure 7), plus GPS coseismic offsets (Figure 7 far left). Maximum slip is limited by coarse slip patches of this model fault.
Green stars are SSN Mexico epicenters for 2018 Pinotepa and 2012 Ometepec quakes. Orange triangles are SSN Mexico epicenters M>=4 from 2018/02/01–11/09. Not all events are near the area of significant slip from M7.2 Pinotepa rupture.
(*Right*) Mean of 150k samples of slip PDF from AlTar run on fault v5 with 10x10 km patches on smaller section of Slab2. Slip vectors shown with 95% error ellipses from PDF of each patch. Same geodetic inputs as v1.2 inversion and along-rake uniform prior, but added rake perpendicular component with prior Gaussian distribution with σ=0.8 m.

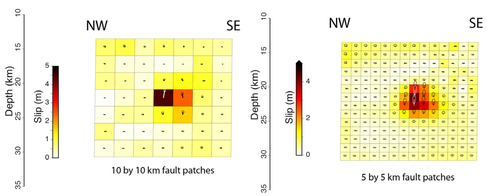

Figure 6. Comparison of effects of changing patch size for same fault area from Slab2 in AlTar slip inversions, plotted looking horizontally at the fault surface so vertical axis is depth and horizontal axis is along-strike distance. Same input datasets and prior slip (uniform along-rake, Gaussian σ=0.8 m rake-perpendicular). Both plots show mean slip of 1 million samples in color scale with direction, magnitude and 95% error ellipses of slip vector calculated from posterior distribution functions of each patch. (*Left*) Model v5 fault with 10x10 km (same as Figure 5 right) patches has very small estimated errors on each patch slip. (*Right*) Model v4 fault with 5x5 km patches has much greater uncertainty of slip on each patch due to trade-offs of slip on adjacent patches. This indicates that surface InSAR data is able to resolve slip on 10 km patches at 22 km depth but not completely resolve slip on 5 km patches. No regularization is applied in AlTar inversions, so width of high slip is controlled only by data and model assumptions (homogeneous elastic halfspace and Slab2). Slip on shallow slip patches has greater uncertainty because patches are offshore.

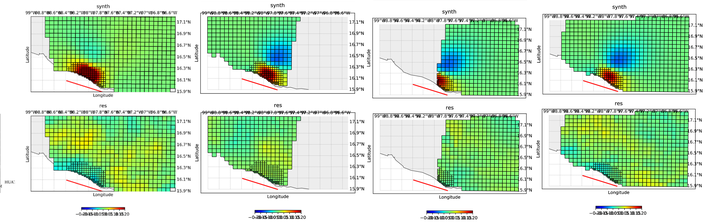

Figure 7. Input InSAR datasets after downsampling (*top row*) from four interferograms. Interferograms were corrected for large-scale tropospheric effects using GACOS (Yu et al., 2017). ALOS-2 interferogram corrected for ionospheric effects (Liang and Fielding, 2017). Downsampling used fault-resolution optimization with fault v4 (Lohman and Simons, 2005) implemented in CSI.

Synthetic surface displacements projected into LOS directions of the four interferograms (*middle row*) from mean slip model of AlTar fault v4 inversion (Figure 6 right). Red line shows location of top edge of the model fault.

Residuals for each interferogram minus the synthetic prediction (*bottom row*). All interferograms have substantial residuals due to tropospheric water vapor variations that are partly correlated with topography in the high coast range mountains of Oaxaca.

far left map shows fit to GPS coseismic offset estimates with data (black) and synthetic (red) horizontal displacement vectors from same model.

2012 Mw 7.4 near Ometepec on megathrust

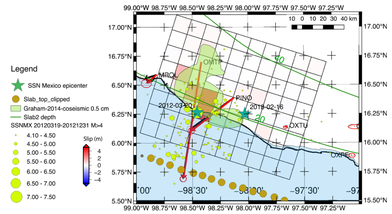

Figure 8. Slip model for 2012 Mw 7.4 Ometepec Earthquake from AlTar inversion of GPS coseismic offsets from Graham et al. (2014). Colored rectangles show mean slip from PDFs of 150,000 slip models (15 x 15 km patches on Slab2 surface, same fault v1.2 as Figure 5). Black arrows show GPS coseismic offsets with estimated uncertainty ellipses and red arrows show prediction from mean slip model. Polygon with green fill shows interpreted slip area greater than 0.5 meters from Graham et al. (2014). AlTar inversion confirms area of high slip in Graham inversion, but not lobe of slip extending over to epicenter of 2018 earthquake. Green circles show aftershocks located by regional SSN Mexico network scaled by magnitude. Green stars show epicenters of 2012 Mw 7.4 Ometepec and 2018 Mw 7.2 Pinotepa quakes.

Slip behavior of Oaxaca-Guerrero megathrust

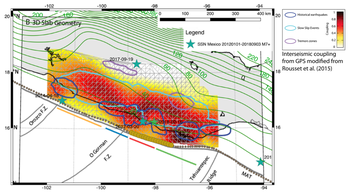

Figure 10. Interseismic coupling model for megathrust beneath Guerrero and Oaxaca estimated from GPS time series (Rousset et al., 2015) shown as colors. This interseismic model used 3D curved megathrust surface from Slab1.0 (Hayes et al., 2012). Polygons with dark blue, cyan and purple outlines show areas of historical earthquakes, slow slip events, and tremor zones (Rousset et al, 2015). Green contours show new Slab2 depth. Green stars show epicenters of 2012 Mw 7.4 Ometepec and 2018 Mw 7.2 Pinotepa quakes from SSN Mexico catalog and purple-filled polygons show their rupture zones from AlTar inversions (this study).

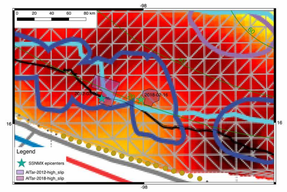

Figure 11. Detail of interseismic coupling model for megathrust beneath Guerrero and Oaxaca estimated from GPS time series (Rousset et al., 2015) shown as colors in area of 2012 Ometepec and 2018 Pinotepa earthquakes (same as Figure 10). Polygons with dark blue, cyan and purple outlines show areas of historical earthquakes, slow slip events, and tremor zones (Roussett et al, 2015). Green contours show Slab2 depth. Green stars show epicenters of 2012 Mw 7.4 Ometepec and 2018 Mw 7.2 Pinotepa quakes from SSN Mexico catalog and purple-filled polygons show their rupture zones from AlTar inversions (this study). Ruptures of 2012 and 2018 quake both fall in area estimated as approximately 50% interseismic coupling. Results of this study suggest this zone has small patches of strong coupling that rupture in earthquakes but may also include areas of slow slip events or creep.

Summary

[1] 2018 Mw 7.2 Pinotepa Earthquake on 16 February was accurately located near city of Pinotepa Nacional by analysis of InSAR data, about 40 km away from preliminary locations based on global teleseismic data alone.

[2] Pinotepa earthquake source was compact, about 10 x 15 km, and ruptured with thrust slip at about 20-22 km depth on the megathrust.

[3] Reanalysis of coseismic GPS offsets for 2012 Mw 7.4 Ometepec Earthquake shows moderate 30 x 30 km slip on megathrust, with no overlap between 2012 and 2018 ruptures.

[4] Both 2012 and 2018 M7 quake ruptures had small areas of high slip, and are located in area previously estimated with roughly 50% interseismic coupling. This zone likely has small patches of full coupling that rupture in M7 earthquakes.

Acknowledgments:
We thank R. Jolivet for the CSI package used for the fault slip modeling and AlTar pre- and post-processing. InSAR processing was done with JPL InSAR Scientific Computing Environment (ISCE) software (Rosen et al., 2012) and Sentinel-1 interferograms were processed by the Advanced Rapid Imaging and Analysis (ARIA) project. Atmospheric corrections were done with the GACOS system Yu et al., 2017) and TRAIN (Bekaert et al., Part of this research was supported by the NASA Earth Surface and Interior focus area and performed at the Jet Propulsion Laboratory, California Institute of Technology. This work contains modified Copernicus Sentinel data from the Sentinel-1A and -1B satellites processed by the European Space Agency (ESA) and JPL. Original ALOS-2 is copyright JAXA (2017) and provided under JAXA RA4 PI Projects P1372002 and P1385002. Some figures were prepared with the Generic Mapping Tools (Wessel et al., 2013) and others with QGIS (QGIS, 2016).

References:

Bekaert, D. P. S., R. J. Walters, T. J. Wright, A. J. Hooper, and D. J. Parker (2015), Statistical comparison of InSAR tropospheric correction techniques, Remote Sens. Environ., 170, 40-47, doi:10.1016/j.rse.2015.08.035.
Graham, S. E., C. DeMets, E. Cabral-Cano, V. Kostoglodov, A. Walpersdorf, N. Cotte, M. Brudzinski, R. McCaffrey, and L. Salazar-Tlaczani (2014), GPS constraints on the Mw = 7.5 Ometepec earthquake sequence, southern Mexico: coseismic and post-seismic deformation, Geophys. J. Int., 199(1), 200-218, doi:10.1093/gji/ggu167.
Hayes, G. P., D. J. Wald, and R. L. Johnson (2012), Slab1.0: A three-dimensional model of global subduction zone geometries, Journal of Geophysical Research: Solid Earth, 117(B1), *n/a-n/a*, doi:10.1029/2011JB008524.
Hjörleifsdóttir, V., S. K. Singh, and A. Husker (2016), Differences in Epicentral Location of Mexican Earthquakes between Local and Global Catalogs: An update, Geofísica Internacional, 55(1), 79-93.
Huang, M.-H., E. J. Fielding, H. Dickinson, J. Sun, J. A. Gonzalez-Ortega, A. M. Freed, and R. Bürgmann (2017), Fault Geometry and Slip Distribution of the 2010 Mw 7.2 El Mayor-Cucapah Earthquake from Geodetic Data, Journal of Geophysical Research, doi:10.1002/2016JB012858.
Minson, S. E., M. Simons, and J. L. Beck (2013), Bayesian inversion for finite fault earthquake source models I-theory and algorithm, Geophys. J. Int., 194(3), 1701-1726, doi:10.1093/gji/ggt180.
QGIS Development Team (2016), QGIS Geographic Information System, edited, Open Source Geospatial Foundation Project.
Rosen, P. A., E. Gurrola, G. F. Sacco, and H. Zebker (2012), The InSAR Scientific Computing Environment, paper presented at 9th European Conference on Synthetic Aperture Radar, Nuremberg, Germany, 23-26 April.
Rousset, B., et al. (2015), Lateral Variations of Interplate Coupling along the Mexican Subduction Interface: Relationships with Long-Term Morphology and Fault Zone Mechanical Properties, Pure Appl. Geophys., 173(10-11), 3467-3486, doi:10.1007/s00024-015-1215-6.
Wessel, P., W. H. F. Smith, R. Scharroo, J. F. Luis, and F. Wobbe (2013), Generic Mapping Tools: Improved version released, Eos Trans. AGU, 94(45), 409-410, doi:10.1002/2013EO450001.
Yu, C., N. T. Penna, and Z. Li (2017), Generation of real-time mode high-resolution water vapor fields from GPS observations, Journal of Geophysical Research: Atmospheres, 122(3), 2008-2025, doi:10.1002/2016JD025753.